Albumin binding, antioxidant and antibacterial effects of cerium oxide nanoparticles

Article *in* Journal of Molecular Liquids · October 2019

DOI: 10.1016/j.molliq.2019.111839

15 authors, including:

Anwarul Hasan
Qatar University

Abbas Salihi
Salahaddin University - Erbil

Nadir Mustafa Qadir Nanakali
Salahaddin University - Erbil

Mudhir Sabir Shekha
Salahaddin University - Erbil

Journal of Molecular Liquids 296 (2019) 111839

Contents lists available at ScienceDirect

Journal of Molecular Liquids

journal homepage: www.elsevier.com/locate/molliq

Albumin binding, antioxidant and antibacterial effects of cerium oxide nanoparticles

Seyedeh Zahra Khoshgozaran Roudbaneh [a, f, 1], Sepideh Kahbasi [b, 1], Mohammad Javad Sohrabi [c], Anwarul Hasan [d, e], Abbas Salihi [f, g], Amir Mirzaie [b], Ali Niyazmand [h], Nadir Mustafa Qadir Nanakali [i, j], Mudhir Sabir Shekha [f, k], Falah Mohammad Aziz [f], Gholamreza Vaghar-Lahijani [l], Aliasghar Bagheri Keshtali [b], Ehsan Ehsani [b, ***], Behnam Rasti [a, **], Mojtaba Falahati [m, *]

[a] Department of Microbiology, Faculty of Basic Sciences, Lahijan Branch, Islamic Azad University (IAU), Lahijan, Guilan, Iran
[b] Department of Biology, Roudehen Branch, Islamic Azad University, Roudehen, Iran
[c] Department of Pharmacology, School of Medicine, Tehran University of Medical Sciences, Tehran, Iran
[d] Department of Mechanical and Industrial Engineering, College of Engineering, Qatar University, Doha, Qatar
[e] Biomedical Research Centre (BRC), Qatar University, 2713, Doha, Qatar
[f] Department of Biology, College of Science, Salahaddin University-Erbil, Kurdistan Region, Iraq
[g] Department of Medical Analysis, Faculty of Science, Tishk International University, Erbil, Iraq
[h] Department of Biology, Faculty of Basic Sciences, Lahijan Branch, Islamic Azad University (IAU), Lahijan, Guilan, Iran
[i] Department of Biology, College of Science, Cihan University- Erbil, Kurdistan Region, Iraq
[j] Department of Biology, College of Education, Salahaddin University-Erbil, Kurdistan Region, Iraq
[k] Department of Pathological Analysis, College of Science, Knowledge University, Erbil, 074016, Kurdistan Region, Iraq
[l] Department of Chemistry, Faculty of Basic Sciences, Lahijan Branch, Islamic Azad University (IAU), Lahijan, Guilan, Iran
[m] Department of Nanotechnology, Faculty of Advanced Sciences and Technology, Tehran Medical Sciences, Islamic Azad University, Tehran, Iran

ARTICLE INFO

Article history:
Received 22 July 2019
Received in revised form
25 September 2019
Accepted 26 September 2019
Available online 9 October 2019

Keywords:
Cerium oxide
Nanoparticle
Albumin binding
Antioxidant
Antibacterial activity

ABSTRACT

Herein, the interaction of CeO_2 NPs with HSA was explored by fluorescence, CD, UV–vis and molecular docking studies. Afterwards, the antioxidant activity of CeO_2 NPs against H_2O_2-induced oxidative stress in BM-MSCs were explored by MTT, ROS and apoptosis assays. Antibacterial assay was also done on two Gram-positive and Gram-negative bacterial strains. Fluorescence study showed that the interaction of CeO_2 NPs with HSA occurs through static quenching and hydrophilic interactions are involved in the spontaneous complex formation. The theoretical study also revealed that the distribution of hydrophilic residues of HSA is dominant in the binding site. CD and UV–vis techniques also revealed that the ellipticity changes and Tm of HSA, respectively did not alter significantly in the presence of CeO_2 NPs. Cellular assays depicted that CeO_2 NPs did not induce cytotoxicity against BM-MSC up to 50 μg/ml for 24 h and pretreatment of cells with CeO_2 NPs can reduce the cell mortality, ROS production and apoptosis in BM-MSC exposed to oxidative stress. The antibacterial assay revealed that CeO_2 NPs have a significant antibacterial effect against all studied bacterial strains. This study may provide useful details about the biomedical applications of CeO_2 NPs.

1. Introduction

Since the appearance of nanotechnology, nanoparticles (NPs) have been wildly implemented as potential agents in biotechnological [1] and medical sciences [2]. NPs encircle a wide number of different materials which supply a high-yielding base for creativity, inventiveness, investigation and buildout. Although, macroscopic materials normally stand in need of remarkable bioactivity due to low biodistribution, and quickly and fully soluble particles usually

* Corresponding author.
** Corresponding author.
*** Corresponding author.
E-mail addresses: e.ehsani@riau.ac.ir (E. Ehsani), rasti@liau.ac.ir (B. Rasti), mojtaba.falahati@alumni.ut.ac.ir (M. Falahati).
[1] These authors contributed equally to this work.

https://doi.org/10.1016/j.molliq.2019.111839
0167-7322/

perform exclusively via chemical reactions, nano-based materials bring into play their function on biological systems through several mechanisms. Furthermore, NPs are considered to be extremely reactive chemically due to their large surface/volume ratio, as well as potential release systems for biologically vital compounds. For example, NPs may be used as an antioxidant agents as well as drug carriers for the delivery of antioxidant enzymes to reduce reactive oxygen species (ROS) [3]. As reported by Gaucher et al., certain NPs may preserve cells by decreasing ROS [3]. Also, it has been revealed that NPs may show potential antibacterial effects against a wide range of bacterial strains [4,5]. Therefore, NPs may form a therapeutic standpoint which may facilitate the development of systems performing through a combination of physical and chemical kinds of interaction. The potency of NPs as drugs is associated with gradually gathering at the area of operation at healing levels, anyhow, challenges such as quick renal clearance, lack of biocompatibility and degradation responses or non-targeted drug delivery make necessary NP delivery qualifying assemblies. Albumin is known as a natural carried protein with several ligand binding positions, cellular receptors, and a long bioavailability [6]. Utilization of these features stimulates albumin as a potential agent for bioavailability extension and selective intracellular delivery of NPs attached by ligand-mediated interactions.

Mesenchymal stem cells (MSCs) therapy can be used against a wide range of disorders [7,8]; however, high levels of ROS derived from the microenvironment of injury site may induce mortality of MSCs [9]. Therefore, NP technology and MSCs therapy can be combined to mitigate the oxidative stress-induced mortality of MSCs [9].

In another view, the spread of antibiotic resistant bacteria has resulted in exploring brand new potential antibacterial candidates [10].

Cerium oxide (CeO_2) NPs have been reported to work as excellent candidate in biological applications [11], nanomedicine [12], antibacterial agents [13], biomedical applications [13], and biosensors [14].

For example, Hirst et al. (2009) [15] and Wason et al. (2013) [16] reported that CeO_2 NPs show anti-inflammatory and anticancer properties, respectively. Recently Bellio et al. (2018) [17] revealed that as CeO_2 NPs can be used as a novel antibiotic adjuvant. Furthermore, Eriksson et al. (2018) [18] demonstrated that CeO_2 NPs possess antioxidant activities and can be employed as a complement agent for MRI contrast.

Although, the antioxidant and antibacterial properties of the NPs have been extensively studied, the simultaneous study of their binding properties to proteins and the calculation of their binding and thermodynamic parameters along with their antimicrobial and antioxidant properties can be of interest. Indeed, when considering the pharmacological properties of NPs, it is important to evaluate all aspects including their interaction with carrier proteins and their medicinal properties such as antioxidant and antibacterial features.

Therefore, we tried to explore the human serum albumin (HSA) binding properties of CeO_2 NPs as well as structural changes of protein after interaction with CeO_2 NPs by biophysical and theoretical approaches. Afterwards, protective impacts of CeO_2 NPs on oxidative stress-induced apoptosis in human bone marrow (BM)-MSCs will be investigated by cellular assays. Finally, the antibacterial effects of CeO_2 NPs against four pathogenic bacteria, including *E. coli* ATCC 25922, *Klebsiella Pneumoniae* ATCC 13883, *Pseudomonas aeruginosa* ATCC 27853 and *Staphylococcus aureus* ATCC 25923 were explored.

2. Materials and methods

2.1. Materials

HSA was obtained from Sigma-Aldrich Company (Sigma-Aldrich, St Louis, MO, USA). CeO_2 NPs (purity: 99.97%, APS: 10–30 nm, SSA: 30–50 m^2/g, color: light yellow, bulk density: ~0.8–1.1 g/cm^3, true density: 7.132 g/cm^3) was purchased from US Research Nanomaterials, Inc. (Houston, TX 77084, USA).

2.2. Methods

2.2.1. Protein and NP preparation

HSA solution was prepared in10 mM phosphate buffer, pH 7.4 and NP solution was dissolved in double-distilled water. NP solution was then sonicated for 20 min at 50 °C employing a sonicator probe (Misonix- S3000, USA). HSA concentration was calculated using the Beer-Lambert equation with an extinction coefficient of 35700 $M^{-1}\,cm^{-1}$ in a UV–vis spectrophotometer. Also, the concentration of CeO_2 was calculated based on the following equation

$$[CeO_2\ NP] = (W/\rho\ V\ v) \tag{1}$$

where, W, ρ, V, and v are weight, density, the volume of a single NP, and final volume of colloidal solution, respectively.

2.2.2. XRD analysis of NPs

The XRD pattern of CeO_2 NPs was investigated by an X-ray diffractometer (PW1730, voltage: 40 kV, current: 30 mA; Philips, Netherlands) at a 2θ in the range of 10–80°.

2.2.3. Intrinsic fluorescence study

Fluorescence spectroscopy was carried out to determine the mechanism of quenching, binding parameters and thermodynamic parameters of Hb after interaction with CeO_2 NPs.

HSA solution with a concentration of 2 μM was titrated with different concentrations of CeO_2 NPs (2–20 μM) and fluorescence spectra (λex: 280 with slit width of 5 nm; λex: 310–450 nm with slit width of 10 nm) were read by Cary Eclipse fluorescence spectrofluorometer (Varian, Australia) at 298 K, 310 K, and 315 K. All spectra were corrected against fluorescence intensities of NP solution, buffer solution, and inner filter effects.

Stern-Volmer equation (2) was used to determine the kind of quenching mechanism based on the following equation (2) [19]:

$$F_0 / F = K_{SV}[NP] + 1 = kq\ \tau 0[NP] \tag{2}$$

where, F, F_o, K_{SV} [NP], kq, and $\tau 0$ represent the fluorescence intensity of HSA incubated with NP, the fluorescence intensity of HSA, Stern-Volmer constant, collision-quenching rate constant, and an average fluorescent lifetime of the macromolecules without NP (10^{-8} s).

Moreover, binding constants [number of binding sites (n) and binding constant (K_b)] were calculated based on the modified Hill equation (3) [19]:

$$\text{Log}\ [F0 - F / F] = n\ \log\ [NP] + \log K_b \tag{3}$$

Furthermore, thermodynamic parameters [enthalpy changes ($\Delta H°$) and entropy changes ($\Delta S°$)] were estimated using the van't Hoff equation (4) [19]:

$$\text{Ln}K_b = -\Delta H°/RT + \Delta S°/RT \tag{4}$$

Finally, the free Gibbs energy ($\Delta G°$) was calculated employing Gibbs-Helmholtz equation (5) [19]:

$$\Delta G^{\circ} = \Delta H^{\circ} - T\ \Delta S^{\circ} \quad (5)$$

2.2.4. Simulation methods

Three spherical nanoclusters with diameters of 1, 2 and 3 nm and a cubic nanocluster with a diameter of 1.5 nm were developed by repeating CeO_2 unit cell [20]. The 3D X-ray crystal conformation of HSA was obtained from the Protein Data Bank (PDB ID: 1AO6). Hex 6.3 (http://hexserver.loria.fr/) as the docking program was utilized to study CeO_2 nanoclusters-HSA interactions [21].

2.2.5. Circular dichroism study

Far UV-Circular dichroism (CD) [(190–260) nm, HSA concentration (200 μg/ml)] was performed by a spectropolarimeter (model 215, Aviv, Lakewood, NJ, USA) with a scan rate of 2 nm/s to determine the secondary structural changes of HSA titrated with different concentrations of CeO_2 NPs (1,10 50 μg/ml). The ellipticity changes of buffer and NP solution was subtracted from the protein signal.

2.2.6. UV–vis study

UV–vis spectroscopy study was performed to determine the melting temperature (Tm) of HSA in the forms of free as well as complex states using a absorbance spectrometer (Varian, Australia). HSA with a concentration of 500 μg/ml was incubated with 50 μg/ml of CeO_2 NPs for 2 min. Afterwards, the absorbance changes of protein samples were read versus a temperature range of 40–90 °C with a scan rate of 1 °C/min. The absorbance of HSA samples was corrected against NP and buffer intensities.

2.2.7. Cell culture

BM-MSCs were obtained from Royan Institute of Tehran, Iran which had been extracted under Ethical approval from Royan Institute Ethics Committee and characterized data for MSC markers and cell culture were provided in Pourgholaminejad et al. (2016) study [22]. Therefore, the cell culture was done based on a previous report [22]. After removing non-adherent cells and reaching confluence, cell treatment was carried out.

2.2.8. Cell treatments and MTT assay

To explore the protective impact of CeO_2 NPs, cells were pretreated with various concentrations of CeO_2 NPs (0.1–50 μg/mL) for 12 h, followed by addition of 200 μM H_2O_2 for 12 h at 37 °C. Cells that did not receive specific treatment were considered as the control group. The viability percent of BM-MSCs was analyzed using the MTT assay based on the previous report [20].

2.2.9. ROS levels

The production of intracellular ROS was examined based on the protocol of DCFDA/H_2DCFDA - Cellular ROS Assay Kit (ab113851). Briefly, following appropriate treatments, the cells were collected, stained with 30 μM of DCFH-DA for 30 min. Afterwards, the fluorescence intensity of the probe was assessed by flow cytometry (FACSCalibur; BD Biosciences, San Jose, CA, USA).

2.2.10. Apoptosis detection by flow cytometry

Annexin V-FITC assay protocol for Annexin V-FITC Apoptosis Staining/Detection Kit (ab14085) was used to quantify the apoptosis and necrosis. After treatment, cells were collected, resuspended in 500 μl of 1× Annexin V binding buffer, stained with 5 μl of Annexin V-FITC and 5 μl Propidium Iodide (PI), and incubated at room temperature for 10 min. Cells were then assessed by flow cytometry (FACSCalibur; BD Biosciences, San Jose, CA, USA).

2.2.11. Agar well diffusion method

In order to evaluation of the antibacterial activity of CeO_2 NPs, agar well diffusion method was used. Briefly, the four pathogenic bacteria including *E. coli* ATCC 25922, *Klebsiella Pneumoniae* ATCC 13883, *Pseudomonas aeruginosa* ATCC 27853 and *Staphylococcus aureus* ATCC 25923 were cultured in LB broth until 0.5 McFarland. Subsequently, each bacterium was coated over the agar plate using sterile cotton swabs. A 6 mm diameter well was punched on Muller Hinton Agar, and various concentrations of CeO_2 NPs (200, 100, 50, 25 μg/mL) was added to each well. After 24 h incubation at 37 °C, the diameter of inhibitory zones measured in mm. Moreover, a concentration of 6 μg/ml of ciprofloxacin was used as a positive control.

2.2.12. Determination of MIC and MBC

In this study, the antibacterial activity of the CeO_2 NPs was also investigated by determination of minimum inhibitory concentration (MIC) and minimum bactericidal concentration (MBC). Briefly, the various concentrations of CeO_2 NPs including 200, 100, 50, 25, 12.5, 6.25, 3.125 and 1.56 μg/mL was prepared and added into the wells. Subsequently, bacterial suspension with 0.5 McFarland was added to each well and incubated at 37 °C for 24 h. The MIC is defined as the lowest concentration that inhibits microbial growth, whereas the MBC was defined as the lowest concentration of antimicrobial agent that can kill 100% of bacteria.

2.2.13. Statistical analyses

Data extracted from control and incubated samples with CeO_2 NPs were statistically analyzed using one-way ANOVA followed by Bonferroni post-hoc test. $P < 0.05$ was considered statically significant.

3. Results

3.1. NP characterization

The morphology and vibrational mode of CeO_2 NPs were fully explored by TEM and FTIR, respectively in our previous paper [20]. Briefly, it was shown that spherical CeO_2 NPs have a diameter of about 30 nm and vibration peaks around 738 cm^{-1}, indicating the presence of pure CeO_2 NPs with a narrow size distribution [20]. Also, to more verify the crystalline structure of CeO_2 NPs, the XRD pattern was determined. As, shown in Fig. 1, the XRD patterns

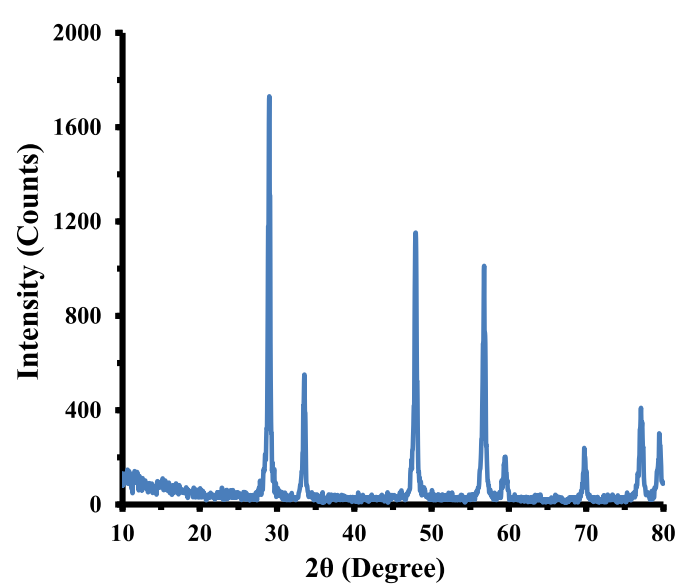

Fig. 1. XRD pattern of the CeO_2 NPs.

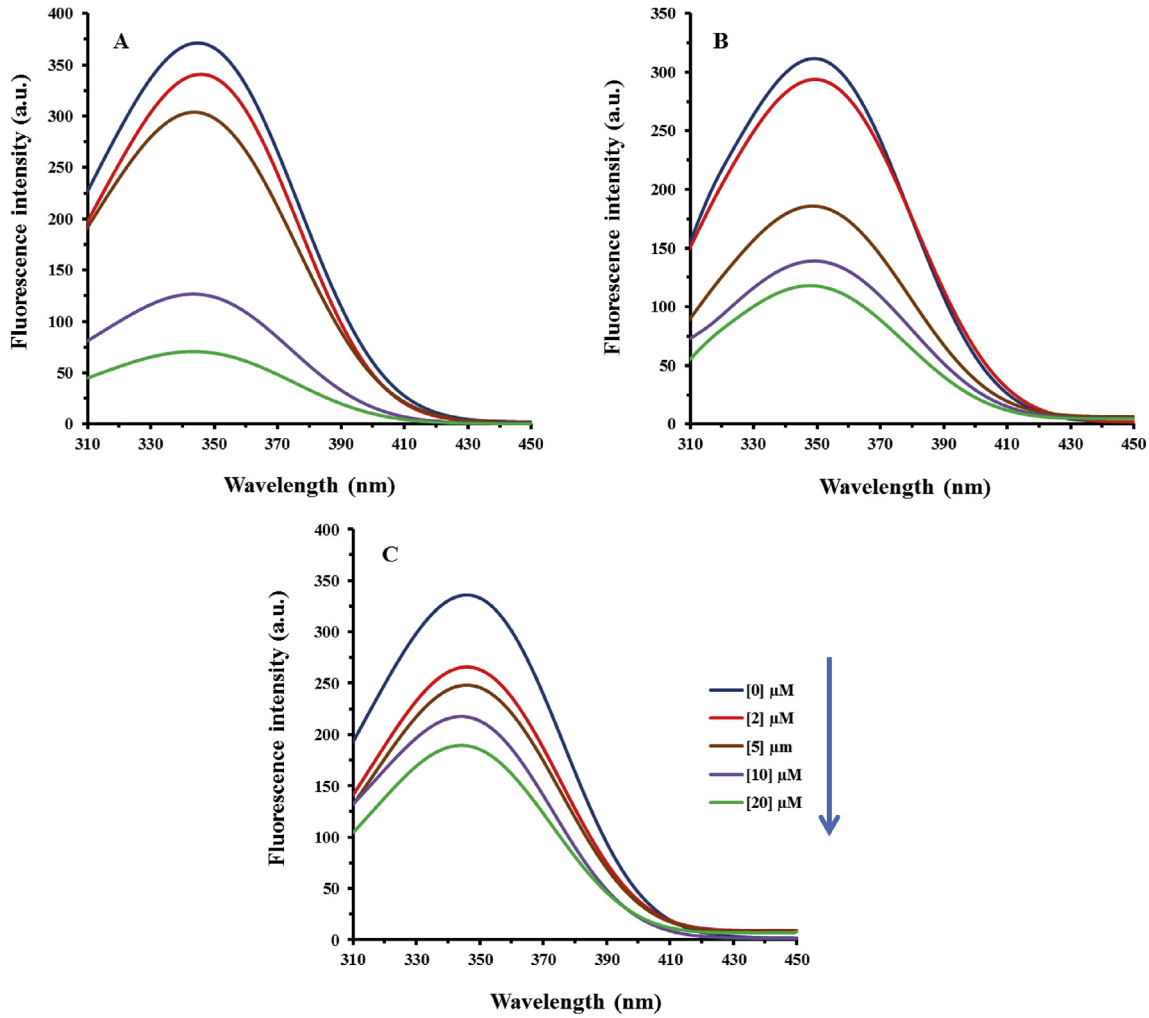

Fig. 2. The fluorescence quenching spectra of free HSA or incubated with varying concentrations of CeO_2 NPs. (A) 298 K, (B) 310 K, and (C) 315 K.

appear at 2θ of 28.99°, 33.51°, 47.92°, 56.79°, 59.49°, 69.80°, 77.06°, 77.31° with different intensities of 1713.84, 509.54, 1139.43, 999.85, 179.93, 184.53, 366.99, and 250.86 counts, respectively. This data is in good agreement with the standard data reported for XRD pattern of CeO_2 NPs.

3.2. Fluorescence quenching of HSA

Fluorescence quenching study can be used to determine the complex specification such as binding constants and thermodynamic parameters [23,24]. Fig. 2 displays the fluorescence quenching of HSA titrated with increasing concentrations of CeO_2 NPs at 298 K Fig. 2A, 310 K Fig. 2B, and 315 K Fig. 2C. This data may represent that aromatic residue may relocate in the protein structure during adsorption of Hb onto the CeO_2 NP surface [25].

K_{SV} and k_q can be calculated to determine the quenching mechanism between NPs and biomolecules. Based on equation (1), the K_{SV} and k_q values for the interaction of CeO_2 NP with HSA deriving from Fig. 3A were calculated and tabulated in Table 1. As summarized in Table 1, the K_{SV} and k_q values at 298 K, 310 K, and 315 K are $2.25 \times 10^5\ M^{-1}$, $8.56 \times 10^4\ M^{-1}$, $3.46 \times 10^4\ M^{-1}$ and $2.25 \times 10^{13}\ M^{-1}\ s^{-1}$, $8.56 \times 10^{12}\ M^{-1}\ s^{-1}$, $3.46 \times 10^{12}\ M^{-1}\ s^{-1}$, respectively. Because K_{SV} values reduce as the temperature of the system increases and k_q is much larger than $10^{10}\ M^{-1}\ s^{-1}$, it may be suggested that the quenching mechanism between CeO_2 NP and HSA occurs through static quenching [26,27].

Also, the F_0 and F presented in Fig. 2 can be used to calculate the binding parameters such as n and K_b based on the Hill equation. Fig. 3B shows the modified Hill plot for the interaction of CeO_2 NP with HSA. The calculated binding parameters are summarized in Table 2.

A larger K_b and n values at 298 K in comparison with higher temperatures reveals the higher level of association between NPs and HSA at a lower temperature. Indeed, these values reduce as the temperature increases, revealing the slight conformational changes induced by temperature, which may displace the interacting residues located at the binding site of HSA with NPs.

The sign of thermodynamic parameters deduced form van't Hoff equation can determine the binding affinity, kind of binding forces and the spontaneity of a reaction.

Fig. 3C shows the van't Hoff plot and the estimated thermodynamic parameters are tabulated in Table 3. The values of ΔS^o and ΔH^o are determined to be −646.56 kJ/mol and −594.10 kJ/mol at room temperature. The negative values of ΔH^o and ΔS^o may designate the formation of van der Waals forces and hydrogen bonding in the adoption position of HSA onto the NP surface [28,29].

3.3. Molecular docking study

The type of interaction between CeO_2 NPs and HSA, which was explored by fluorescence investigation, was further verified by

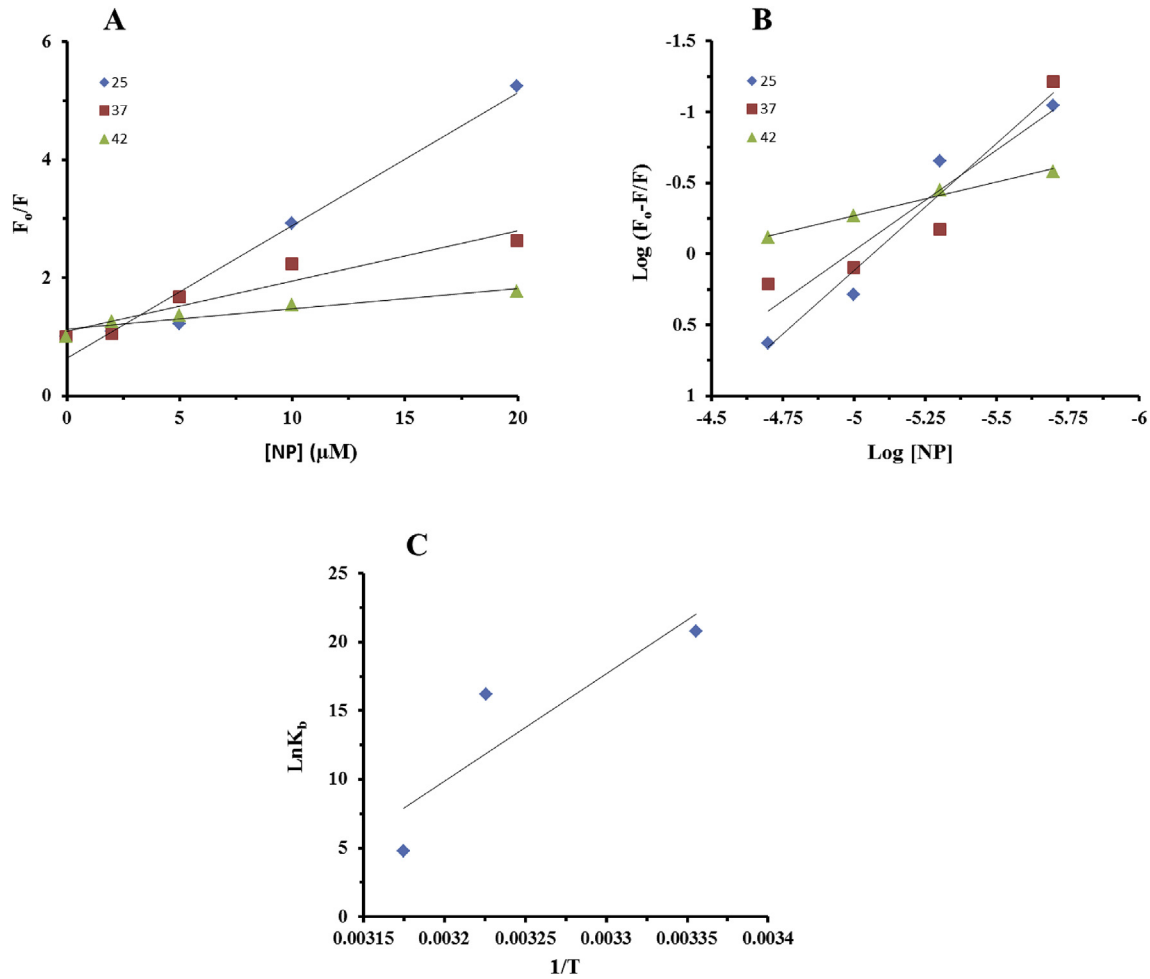

Fig. 3. (A) Stern–Volmer plots, (B) Modified Hill plot, and (C) van't Hoff plot for the interaction of HSA with CeO_2 NPs.

molecular docking study, which results in providing useful details regarding interaction residues and preferable binding sites. To compare the effect of size and morphology of CeO_2 nanoclusters on their affinities to bind HSA, at first three spherical clusters with different sizes and a cubic nanocluster with a size of 1.5 nm were developed by the repetition of CeO_2 unit cell [20]. Afterwards, the cluster/HSA interaction was done by Hex 6.3 program for all designed cluster models. The interaction analysis for 3 spherical nanoclusters with dimensions of 1 nm (Fig. 4A), 2 nm (Fig. 4B) and 3 nm (Fig. 4C) and a cubic nanocluster with the size of 1.5 nm (Fig. 4D) gives binding energies of −277.70 E-value, −444.89 E-value, −67.65 E-value, and −831.41 E-value, respectively (Table 4). Stand on the highest binding energy, cubic nanocluster with the size of 1.5 after interaction with HSA shows preferable binding in comparison with other nanoclusters.

Fig. 5 shows the residues surrounding the spherical CeO_2 nanocluster with dimensions of 1 nm (Fig. 5A), 2 nm (Fig. 5B) and a cubic nanocluster with the size of 1.5 nm (Fig. 5C) within 4 Å explored by using graphical tools. Furthermore, all residues in the binding sites are summarized in Table 4. It is evident from Table 4, the binding energy of cubic nanocluster is remarkably more negative than other nanoclusters, and this nanocluster interacts with Ser-435.B, Glu-400.B, Gly-399.B, Glu-294.A, Cys-289.A, Glu-188.A, Asp-187.A, Glu-292.A, Lys-444.B, His-440.A, Lys-439.B, Lys-436.A, Ser-435.residues. Therefore, this data may assign that hydrogen bonding and van der Waals interactions are playing a main role in the complex formation between CeO_2 NPs and HSA, and this is in agreement with the thermodynamics data derived from fluorescence spectroscopy experiment.

3.4. Circular dichroism study

The circular dichroism (CD) spectroscopy can be employed to explore the structural alterations of free biomolecules or incubated with ligands [19,30] based on the ellipticity changes. Indeed, the CD technique is helpful to determine the probable impact of the interaction action on the secondary structure of the biomolecules. HSA demonstrates in the UV region at 208 and 222 nm two minima,

Table 1
K_{SV} and k_q values for the interaction of CeO_2 NPs with HSA.

T (K)	K_{SV} (M^{-1})	k_q (L $mol^{-1}s^{-1}$)	R^2
298	2.25×10^5	2.25×10^{13}	0.97
310	8.56×10^4	8.56×10^{12}	0.91
315	3.46×10^4	3.46×10^{12}	0.91

Table 2
K_b and n values for the interaction of CeO_2 NPs with HSA.

T (K)	n	LogK_b (M^{-1})	R^2
298	1.78	9.04	0.96
310	1.41	7.05	0.90
315	0.47	2.09	0.99

Table 3
Thermodynamic parameters of the HSA/CeO_2 NPs complex.

T (K)	ΔG° (kJ/mol)	ΔH° (kJ/mol)	$T\Delta S^\circ$ (kJ/mol)
298	−52.45	−646.56	−594.10
310	−40.61		−605.95
315	−12.67		−633.88

Also, the negative value of ΔG^o proposed that the absorption of HSA molecules onto the CeO_2.
NP surface occurs spontaneously.

corresponding to the α-helical conformation of this macromolecule [31]. CD study executed in the presence of increasing concentrations of NPs showed that the binding of CeO_2 NPs to HSA did not lead to a significant reduction in ellipticity (Fig. 6). The CD data were formulated based on the mean residue ellipticity (MRE) in deg cm^2 $dmol^{-1}$, as reported by the following equation (6) [19].

$$\mathrm{MRE} = \text{Observed CD (mdeg)} / \mathrm{C_p}\ \mathrm{nl} \times 10 \tag{6}$$

where Cp shows the molar concentrations of the biomolecule, n represent the total of building block and l is the path length.

The α-helix contents of free and complex HSA were estimated from mean residue ellipticity changes at 222 nm using the following equation (7) [19]:

$$\alpha - \text{helix\%} = \mathrm{MRE}_{222} - 2340/30300 \times 100 \tag{7}$$

Therefore, it was estimated that the reduction of α-helical content is about 0.7%, 1.2% and 1.7% for HSA in the presence of 1 μg/ml, 10 μg/ml and 50 μg/ml CeO_2 NPs, respectively.

3.5. Melting temperature measurement

The UV–vis spectroscopy can be utilized to calculate the Tm value of biomolecules in terms of absorbance changes versus temperature [32]. The UV–vis technique is serviceable to find out the expected influence of the reaction approaches on the structural destabilization of the proteins. Plotting first derivative of absorbance versus temperature also can be used to calculate the Tm values. As shown in Fig. 7, the absorbance of free HSA and HSA complex at 280 nm increases as temperature goes up. Fig. 7 (inset) also represent that both free HSA and interacted one show Tm value of around 70 °C nm, determining the preservation of HSA conformation even after interaction with CeO_2 NPs.

Initially, the influences of CeO_2 NPs with different concentrations of 0.1 μg/ml, 1 μg/ml, 10 μg/ml, 20 μg/ml and 50 μg/ml on BM-MSCs viability for 24 h was examined using the MTT assay. As shown in Fig. 8, treatment of cells with different concentrations of CeO_2 NPs for 24 h influenced little effect on cell viability in

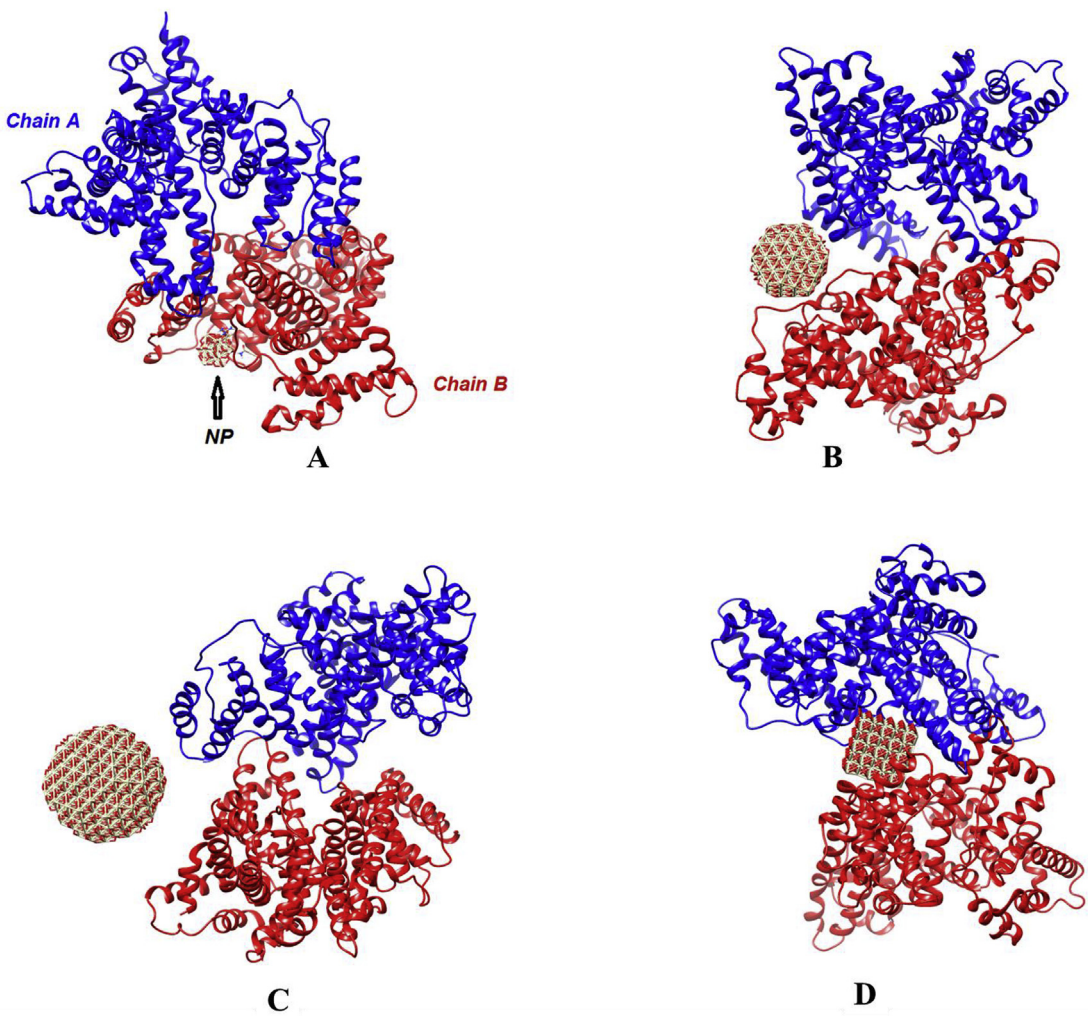

Fig. 4. The molecular binding interaction between HSA and three spherical nanoclusters with different size of (A) 1 nm, (B) 2 nm, (C) 3 nm, and (D) A cubic nanocluster with the size of 1.5 nm.

Table 4
Docking outcomes of CeO_2 nanoclusters with HSA.

Morphology	Diameter (nm)	Docking score (E-value)	Residue interacted
Spherical	1	−277.70	Arg-114.B, Leu-112.B,Asn-109.B,Thr-442.B,Pro 421.B
Spherical	2	−444.89	Glu-294.B, Ala-443.B,Glu-442.B,Pro-441.B, Gln-397.A, Glu-393.A
Spherical	3	−67.65	_
Cubic	1.5	−831.41	Ser-435.B, Glu-400.B, Gly-399.B, Glu-294.A, Cys-289.A, Glu-188.A, Asp-187.A, Glu-292.A, Lys-444.B, His-440.A, Lys-439.B, Lys-436.A, Ser-435.A

comparison with the control group. This data determined that CeO_2 NPs did not trigger cytotoxic effects on BM-MSCs up to 50 μg/ml for 24 h. Therefore, CeO_2 NPs with a concentration of 50 μg/ml was used to study the antioxidant effect of CeO_2 NPs on H_2O_2-induced oxidative stress in BM-MSCs.

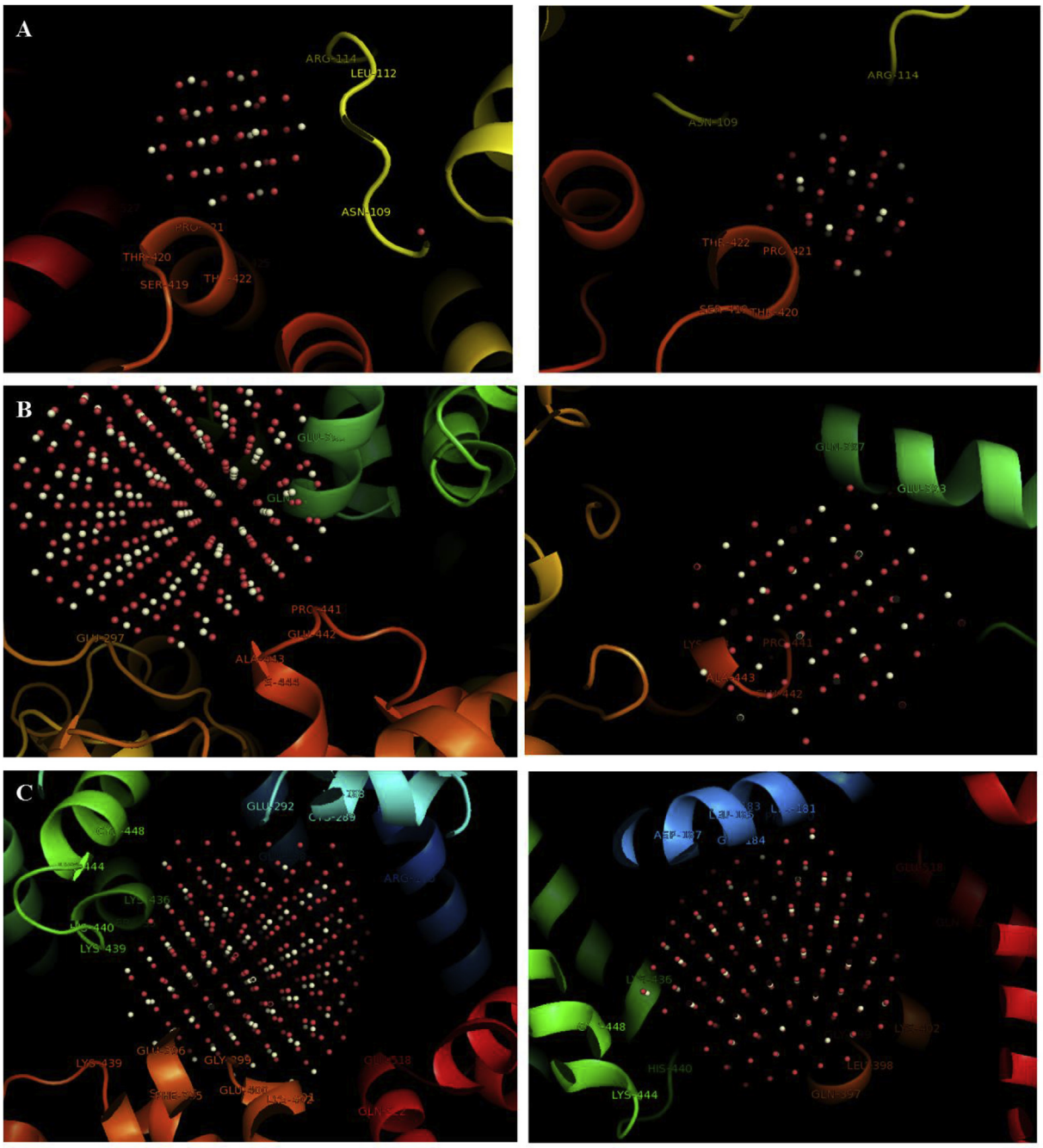

Fig. 5. Analysis of HSA residues contributed in the binding site with spherical CeO_2 nanocluster with dimensions of (A) 1 nm, (B) 2 nm, and (C) A cubic nanocluster with the size of 1.5 nm within 4 Å at two rotational angles..

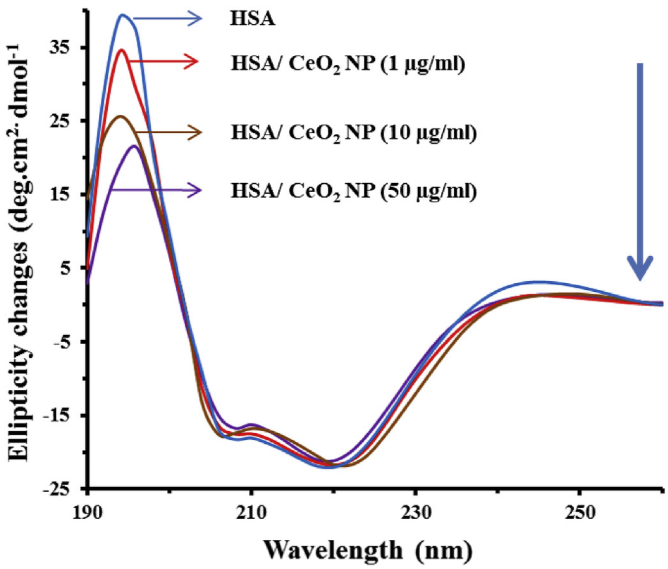

Fig. 6. CD bands of free HSA and HSA/CeO_2 NPs complex with various concentrations of NPs at room temperature.

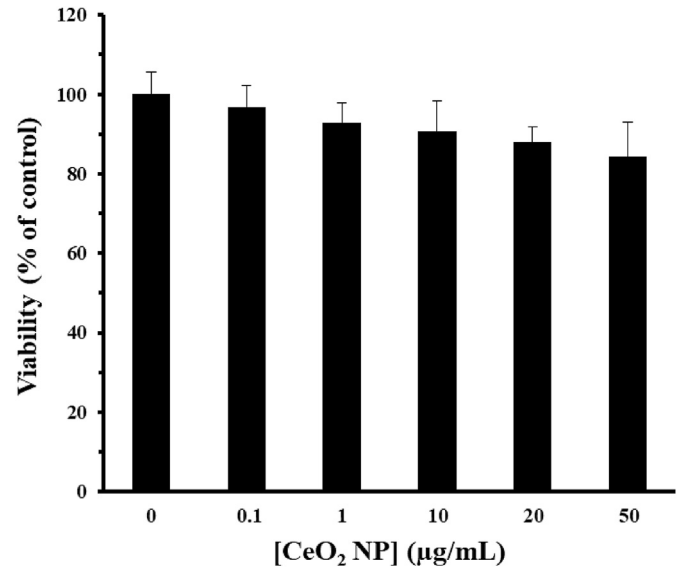

Fig. 8. MTT assay of BM-MSCs in the presence of varying concentrations of CeO_2 NPs (0.1–50 µg/ml) for 24 h.

3.6. CeO_2 NPs significantly inhibits H_2O_2-induced cell mortality of BM-MSCs

H_2O_2 has been shown to trigger cell mortality at different concentrations and time-intervals [20,21]. In this study, following treatment of cells with a single concentration of H_2O_2 (200 µM) for 12 h or CeO_2 NPs with different concentrations of 1 µg/ml, 10 µg/ml, 20 µg/ml and 50 µg/ml followed by H_2O_2 for 12 h, we performed MTT assay. As shown in Fig. 9, BM-MSCs incubated with H_2O_2 had profoundly lower cell viability ($^{***}P < 0.001$, relative to control group) in comparison with BM-MSCs protected by CeO_2 NPs with different concentrations of 10 µg/ml ($^{\#}P < 0.05$, relative to H_2O_2-treated group), 20 µg/ml ($^{\#}P < 0.05$, relative to H_2O_2-treated group) and 50 µg/ml ($^{\#\#}P < 0.01$, relative to H_2O_2-treated group).

3.7. CeO_2 NPs remarkably mitigates H_2O_2-induced ROS production of BM-MSCs

H_2O_2 treatment can result in the intracellular ROS elevation of different cells. To further examine the influences of the CeO_2 NPs against ROS production in H_2O_2-triggered BM-MSCs, we carried out the DCFH-DA staining test. As displayed in Fig. 10A, the DCFH intensity was around 103 unit in the negative control group, whereas we observed that H_2O_2 incubation increased the level of ROS production in BM-MSCs from 103 to 544 unit (Fig. 10B). However, pretreatment with the CeO_2 NPs (50 µg/ml) for 12 h led to a remarkable reduction in the level of ROS production (Fig. 10C). These data represented that H_2O_2 treatment significantly enhanced the level of ROS production ($^{***}P < 0.001$, relative to control group), nevertheless, CeO_2 NPs with a concentration of 50 µg/ml potentially

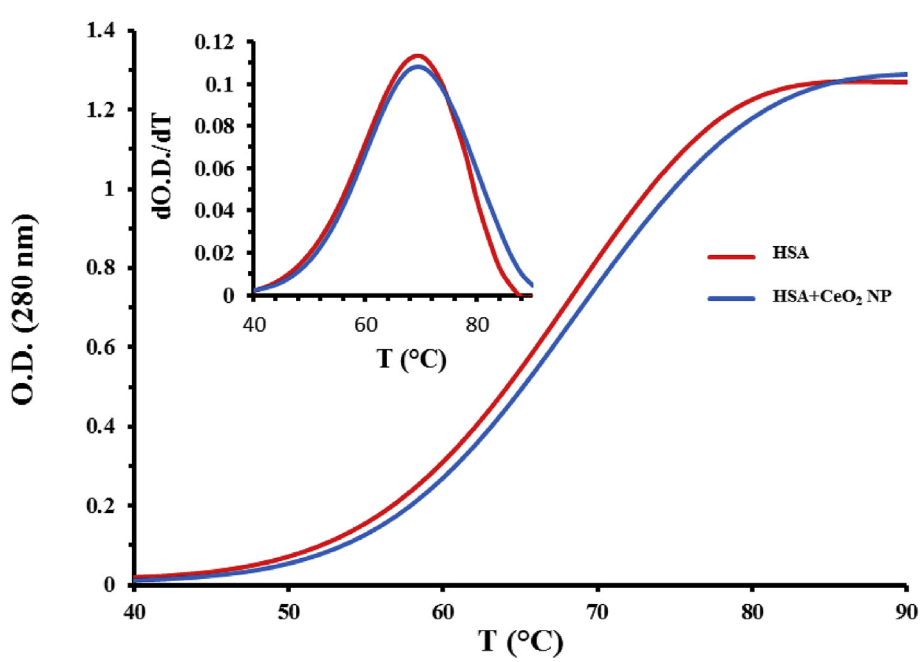

Fig. 7. Thermal profile of free HSA and HSA/CeO_2 NPs (50 µg/ml). The inset shows the first derivative of O.D. versus T.

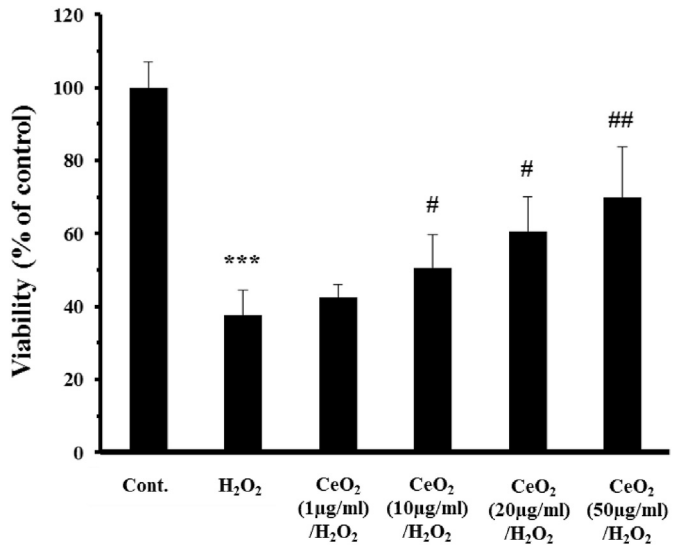

Fig. 9. Influence of CeO_2 NPs on BM-MSCs viability in H_2O_2-triggered oxidative stress. $^{***}P < 0.001$ versus control, $^{\#}P < 0.05$ and $^{\#\#}P < 0.01$ versus H_2O_2 treated cells.

declined the intracellular ROS generation in BM-MSCs treated with H_2O_2 ($^{\#\#}P < 0.01$, relative to H_2O_2-treated group) (Fig. 10D).

3.8. CeO_2 NPs outstandingly reduces H2O2-induced apoptosis of BM-MSCs

To further explore the protective impact of CeO_2 NPs against apoptosis in H_2O_2-induced BM-MSCs, flow cytometry assay was performed. After treatment of BM-MSCs with a single concentration of H_2O_2 (200 μM) for 12 h or CeO_2 NPs with a concentration of 50 μg/ml followed by addition of H_2O_2 for 12 h, BM-MSCs were stained with Annexin V-FITC/PI. The proportion of early apoptotic cells, late apoptotic cells, and necrotic cells were 4.88%, 4.37%, 5.38% (Fig. 11A), 4.46%, 32.42%, 29.61% (Fig. 11B), 3.66%, 9.31%, 6.92% (Fig. 11C), in control cells, H_2O_2-treated cells and H_2O_2-treated cells pre-incubated with CeO_2 NPs (50 μg/ml), respectively. As shown in Fig. 11D, the late apoptosis ($^{***}P < 0.001$, relative to control group) and necrosis ($^{***}P < 0.001$, relative to control group) were significantly enhanced following incubation with 200 μM H_2O_2. However, pre-treatment of cells with CeO_2 NPs results in a reduction of late apoptosis ($^{\#\#\#}P < 0.001$, relative to H_2O_2-treated cells) and necrosis ($^{\#\#\#}P < 0.001$, relative to H_2O_2-treated cells).

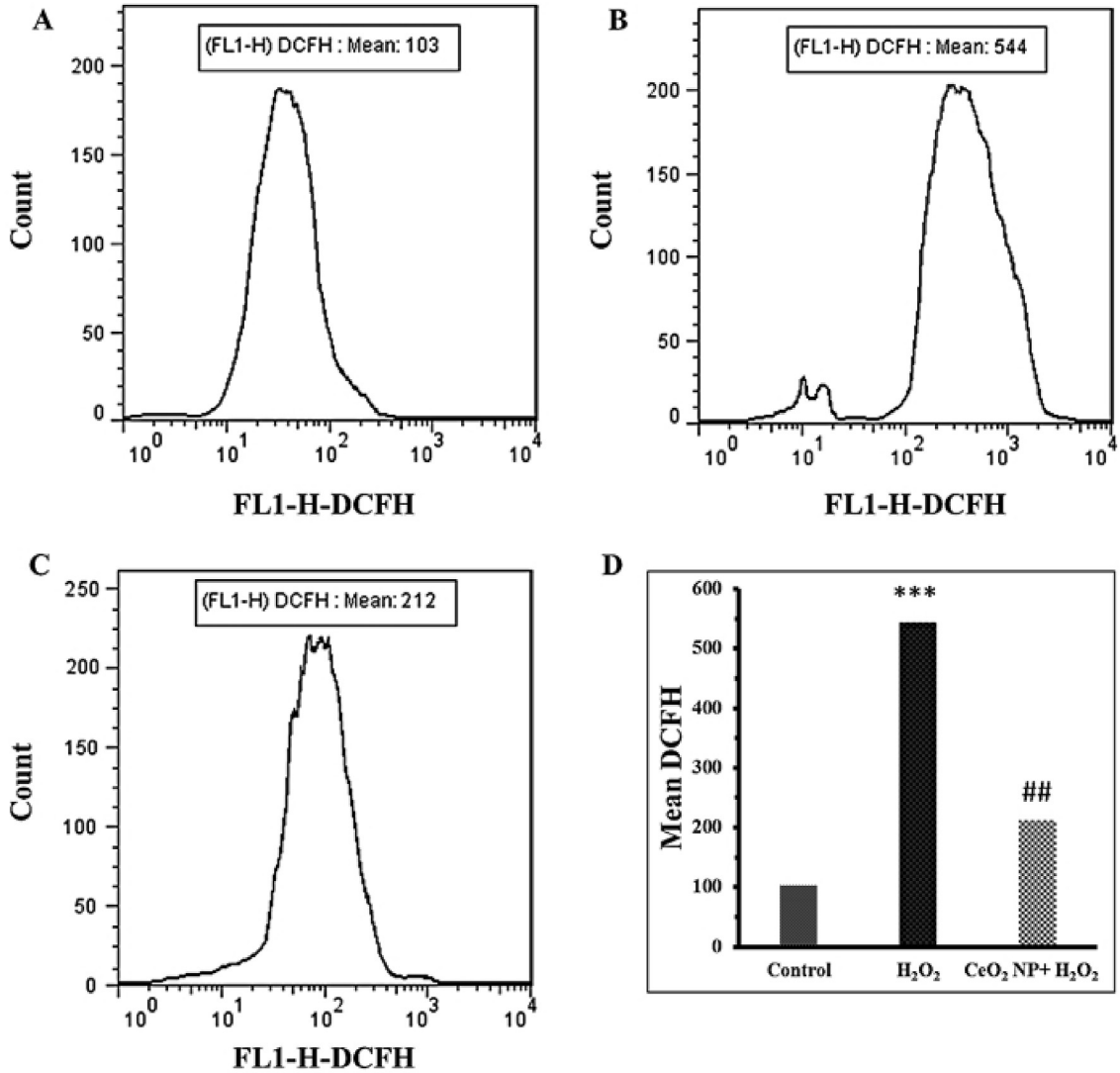

Fig. 10. Protective effect of CeO_2 NPs on intracellular ROS production in BM-MSCs exposed to H_2O_2. Cells were exposed to H_2O_2 (200 μM, for 12 h) after pretreatment with the CeO_2 NPs (50 μg/mL) for 12 h. The ROS production was measured by the DCFH assay. (A) Control cells, (B) H_2O_2-treated cells, (C) Pretreated cells by CeO_2 NPs followed by addition of H_2O_2, and (D) Statistical analysis of ROS assay. $^{***}P < 0.001$ versus control and $^{\#\#}P < 0.01$ versus H_2O_2 treated cells.

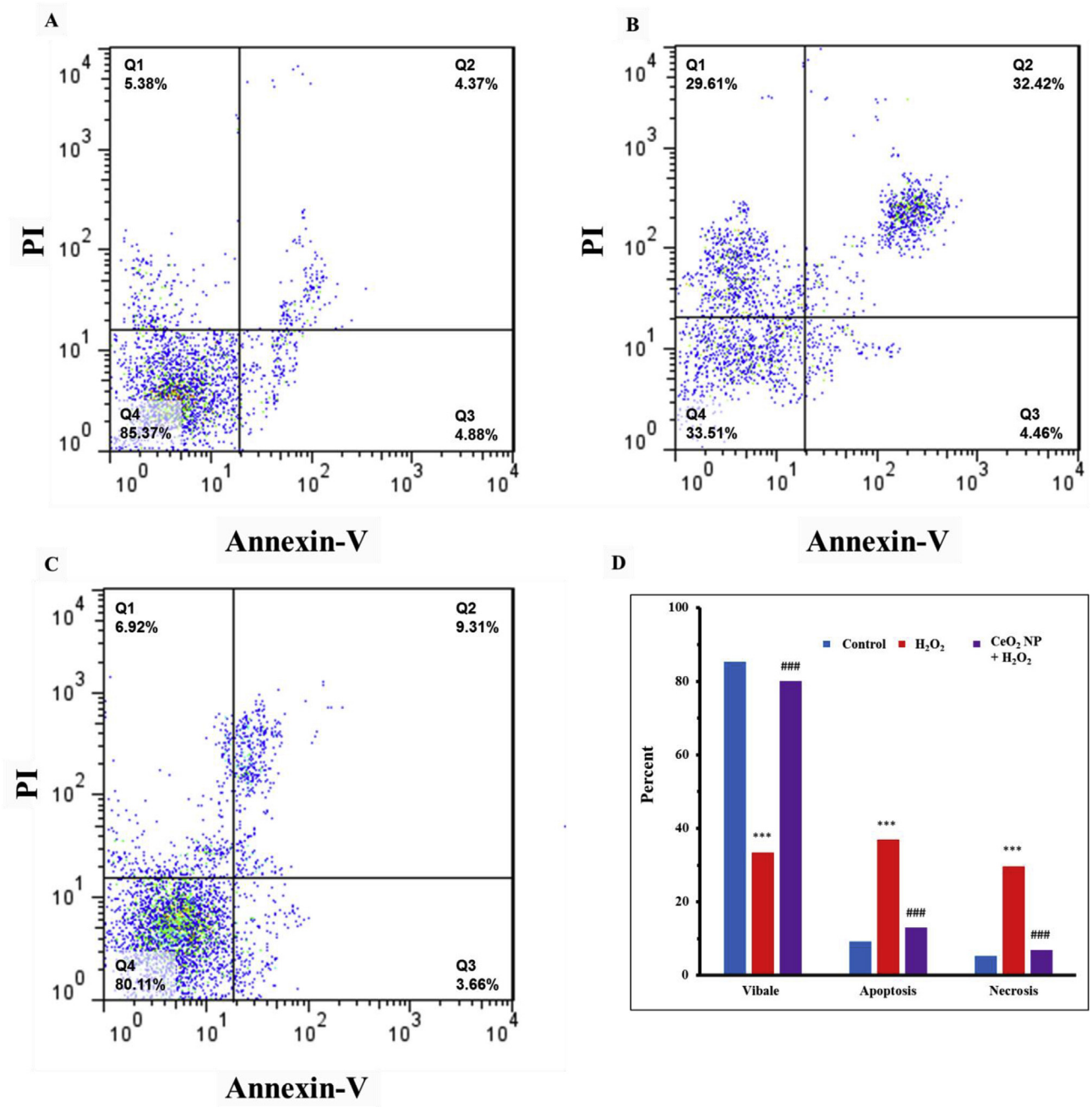

Fig. 11. Antiapoptotic effect of CeO_2 NPs on apoptosis induction in BM-MSCs exposed to H_2O_2. Cells were exposed to H_2O_2 (200 μM, for 12 h) after pretreatment with the CeO_2 NPs (50 μg/mL) for 12 h. The quantification of apoptosis was calculated by the Annexin-V/PI assay. (A) Control cells, (B) H_2O_2-treated cells, (C) Pretreated cells by CeO_2 NPs followed by addition of H_2O_2, and (D) Statistical analysis of apoptosis assay. $^{***}P < 0.001$ versus control and $^{###}P < 0.001$ versus H_2O_2 treated cells.

3.9. Antibacterial activity by well diffusion method

Antibacterial activity of CeO_2 NPs is depicted in Fig. 12. The results show that the CeO_2 NPs had antibacterial activity against selected bacteria. Table 5 shows the inhibition zone diameter (millimeter) of CeO_2 NPs against *S. aureus*, *E. coli*, *P. aeruginosa,* and *K. pneumoniae* strains. As we can observe, inhibition zone of CeO_2 NPs was depending on their concentrations and the large inhibition zone was related to 200 μg/mL concentration for all bacteria. Among them, at the same concentration (200 μg/mL), the largest inhibition zone was related to *E. coli* and *S. aureus* (37 ± 0.5 mm). In addition, at the concentration of 6 μg/ml of ciprofloxacin, *P. aeruginosa* and *S. aureus* had no inhibition zone, whereas other bacteria showed inhibition zone in the same concentration

3.10. MIC and MBC methods

In this study, the antibacterial activity of CeO_2 NPs was also determined using other approaches, MIC and MBC methods. The CeO_2 NPs were shown to be more effective against *E. coli* in comparison with other strains. The MIC and MBC values (μg/mL) of CeO_2 NPs against studied bacteria are shown in Table 6. Based on the results, the CeO_2 NPs showed a very profound antibacterial activity against both Gram-positive and Gram-negative bacteria at very low concentrations.

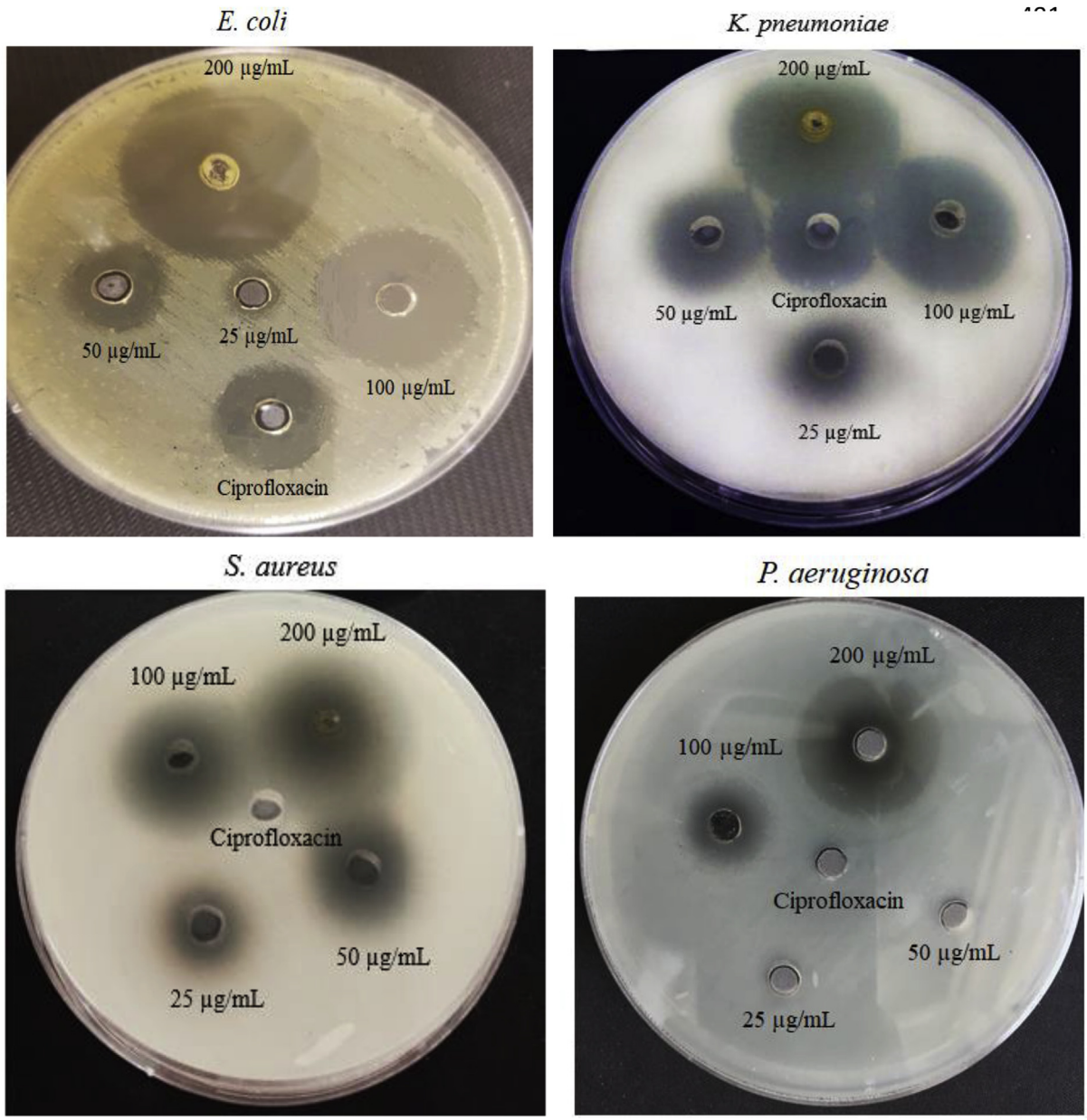

Fig. 12. Inhibition zone induced by CeO_2 NPs against *S. aureus*, *K. pneumoniae, E. coli*, and *P. aeruginosa* strains.

4. Discussion

In this study, we showed by fluorescence spectroscopy that some environmental changes around aromatic residues may occur upon the interaction of HSA with CeO_2 NP. Also, quenching type was deduced to be based on the static quenching. Binding constant such as n and K_b were calculated, and it was concluded that temperature might influence the binding affinity of protein toward NPs.

Thermodynamic parameters were also estimated, and it was demonstrated that hydrophilic interaction are involved in the formation of CeO_2 NP/HSA complex.

Theoretical studies also represented that CeO_2 nanocluster with different morphologies and diameters can interact with different residues on the HSA structure. However, the distribution of hydrophilic residues was more dominant in the binding site, which is in agreement with fluorescence data.

Song et al. (2011) [33] showed that fullerene NPs with the diameter of around 50–110 nm interact with HSA through static quenching, and some environmental changes occur around aromatic residues. Furthermore, Huang et al. (2015) [34] displayed that graphene-quantum dots (QDs) with the size of 1.2 nm result in the formation of a static complex with HSA and establish some hydrophilic interactions with HSA residues. However, it was revealed that the reaction forces upon the interaction of cadmium telluride-QDs with the dimension of around 5 nm and HSA are electrostatic interaction [35].

Regarding the CD and UV–visible sturdy, we demonstrated that CeO_2 NPs did not perturb the secondary structure of HSA and Tm of protein incubated with CeO_2 NPs was almost similar to free HSA.

Treuel et al. (2010) [36] also demonstrated that citrate-functionalized gold (Au) and silver (Ag) NPs provide much stronger interactions and structural changes with bovine serum albumin (BSA) than polymeric or polymer-coated counterparts.

Ansari et al. (2018) [37] also depicted that bare and surface functionalized titanium oxide NPs did not alter the structure of HSA.

Table 5
Average inhibition zone of CeO_2 NPs.

Bacteria	Concentration of CeO_2 NPs (μg/mL)	Inhibition zone (mm)
S. aureus	200	37 ± 0.5
	100	31 ± 0.5
	50	20 ± 1.00
	25	15 ± 0.5
	Ciprofloxacin	–
E. coli	200	37 ± 0.5
	100	31 ± 1.00
	50	18 ± 0.5
	25	4 ± 1.00
	Ciprofloxacin	21 ± 0.5
P. aeruginosa	200	25 ± 0.5
	100	15 ± 1.00
	50	–
	25	–
	Ciprofloxacin	–
K. pneumoniae	200	35 ± 0.5
	100	28 ± 1.00
	50	23 ± 0.5
	25	–
	Ciprofloxacin	21 ± 0.5

Moreover, Maji et al. (2019) [38] reported that bio- Ag NPs may induce some slight changes in the HSA and hemoglobin structure and may be used as potential antibacterial agents in medicine. However, Ambika et al. (2015) [39] exhibited that bio-fabricated zinc oxide (ZnO) NPs may result in secondary structural changes of HSA. Ali et al. (2015) [40] also depicted that interaction of HSA with Ag NP coated with polyvinylthiol cause secondary structural alternations of protein. Moreover, Navvenraj et al. (2018) [41] reported that (nickel, copper, Zn) selenide NPs show different affinity and interaction with HSA and induce some structural changes. Shcharbin et al. (2018) [42] suggested that functional moieties and the core of capped Au NPs may influence their interaction with HSA. Therefore, it should be noted different parameters affect the kind of interaction between NPs and proteins and corresponding structural changes of biomolecules.

Regarding cellular (antioxidant) assays, it was indicated that CeO_2 NPs did not induce significant cytotoxicity against BM-MSCs up to 50 μg/ml for 12 h. Also, CeO_2 NPs can mitigate the cell mortality, ROS production and apoptosis in H_2O_2-induced oxidative stress in BM-MSCs. Rather et al. (2018) [43] also revealed that CeO_2 NPs capped with polycaprolactone -gelatin fibers can be utilized as promising antioxidant agents for wound healing implementations. Moreover, Xue et al. (2018) [44] showed that pegylated CeO_2 NPs could serve as an excellent antioxidant candidate. Furthermore, Patel et al. (2018) [45] displayed that CeO_2 NPs can cross the cell membrane of human monocytic leukemia cells and trigger significant antioxidant activity.

Abuid et al. (2019) [46] also depicted that CeO_2 NPs can be used as coating particles for antioxidant preservation of encapsulated Beta cells. Filippi et al. (2019) [47] showed that morphology of CeO_2 NPs can play a key role in their antioxidant activity and proposed that CeO_2 nanorods provide higher antioxidant activity than CeO_2 NPs. It has also been revealed that antioxidant properties of CeO_2 NPs can be considered as a potential point in hemostasis [48], skin tissue engineering [49], regulation of oxidative markers [50], photoprotection [51], bone regeneration [52], and diabetic wound healing [53]. It may be indicated that the mechanism of antioxidant properties of NPs like CeO_2 is due to the oxidase [54] and superoxide dismutase-like activity of NPs [55]. Indeed, it has been widely shown that NPs can be considered as nonozymes in the biological systems, where they can serve as antioxidant agents to catalyze the conversion of free radicals into non-toxic agents [56–59].

Table 6
MIC and MBC of CeO_2 NPs against pathogenic bacteria. The data were reported as mean ± SD of the three independent experiments.

Bacteria	MIC (μg/mL)	MBC (μg/mL)
S. aureus	25 ± 0.0	50 ± 14.43
E. coli	6.25 ± 3.6	12.5 ± 0.0
P. aeruginosa	12.5 ± 0.0	25 ± 14.43
K. pneumoniae	12.5 ± 3.6	25 ± 0.0

The results of this study also showed that the CeO_2 NPs had significant antibacterial activity against both Gram-positive and Gram-negative bacteria, with more pronounced antibacterial activity against Gram-negative strains (*E. coli*).

There are limited studies about the evaluation of the antibacterial activity of CeO_2 NPs. According to Zeyons et al. [60], Pelletier et al. [61], and Kuang et al. [62], CeO_2 NPs have antibacterial activity against *E. coli*. Moreover, Gopinath et al., reported that the antibacterial activity of CeO_2 NPs in Gram-positive bacteria is due to teichoic acid in peptidoglycan [63].

The MIC of CeO_2 NPs was observed at 25 μg/mL for *S. aureus*, 6.25 μg/mL for *E. coli*, 12.5 μg/mL for both of *P. aeruginosa* and *K. pneumoniae*. The higher antibacterial activity of CeO_2 NPs against *E. coli* comparing to other bacterial strains may be due to different structure and thickness of cell wall. Moreover, based on the well diffusion results, it can be concluded that the antimicrobial activity of CeO_2 NPs is concentration dependent, whereas, at the concentration of 6 μg/ml of ciprofloxacin, *P. aeruginosa* and *S. aureus* had no inhibition zone, whereas other bacteria showed inhibition zone in the same concentration. It appears that *P. aeruginosa* and *S. aureus* are intrinsically resistant to this concentration of ciprofloxacin. One of the reasons for more antimicrobial activity of CeO_2 NPs against Gram-negative bacteria is due to the variation in the thickness of the peptidoglycan in these bacterial strains [64]. Another antibacterial mechanism of CeO_2 NPs is the binding of CeO_2 NPs to the surface of the cell membrane that changes the permeability and respiration of bacteria [60]. Also, in oxi-reduction process, the reduction of Ce^{4+} to Ce^{3+} occurs, resulting in oxidative stress on lipids and proteins in the plasma membrane of cells [56]. Also, some studies reported that the CeO_2 NPs attack to electron flow and bacterial respiration and cause impairment of cellular respiration [60–64].

Besides CeO_2 NP, the antibacterial activity of other NPs such as ZnO NPs [65], titanium oxide NPs [66], nickel oxide NPs [67], copper oxide NPs [68], and Ag NPs [69] have been reported recently.

It has been showed that NPs generate significant level of ROS as the major cause of antibacterial activity [70]. Such reactive species cause destruction of cellular components such as lipids, DNA and proteins as a result of entry to bacterial cells [71]. The another antibacterial mechanism of NPs has been shown to be due to the release of ions which provides a dramatic effect on inhibition of active transport, amino acid metabolism and enzyme disruption [72,73]. The cell energy also decreases in cells following treatment to NPs due to decline in the ATP levels [74,75]. Moreover, NPs with different physicochemical properties can disrupt the membrane integrity causing membrane dysfunction [76].

Also, metal NPs usually carry positive charges which result in an electromagnetic attraction between bacteria and the surface of metal NPs [77]. This attraction leads to oxidation and antibacterial effects of NPs [78].

According to the results, it can be concluded the CeO_2 NPs have the greater antibacterial activity against Gram-negative bacteria in comparison with Gram-positive strains, and it can be used as a drug candidate in future.

Therefore, it may be indicated that CeO_2 NPs can hold a great promise in regulating oxidative stress in injured tissues as well as potency materials for the development of antibacterial agents. However, it should be emphasized that some reports regarding the

toxicity of CeO_2 NPs have been reported [79,80]. Hence, more detailed research should be carried out to explore the mechanism of cytotoxicity, antioxidant activity and antibacterial effects of CeO_2 NPs.

5. Conclusion

In this study, the interaction HSA and CeO_2 NPs was explored by several spectroscopic techniques as well as molecular docking investigation. It was depicted that HSA interacts with CeO_2 NPs to form a stable static HSA-CeO_2 NPs complex. Also, fluorescence data suggested that the interaction of CeO_2 NPs with HSA is spontaneous, and the dominant involving forces are hydrogen bonding and van der Waals interactions. Furthermore, it was determined that secondary structure and Tm of HSA did not change when incubated with CeO_2 NPs. Additionally; the docking study revealed that nanoclusters with different sizes and morphologies could bind to HSA with different affinities. In the cellular assays, we found that CeO_2 NPs can mitigate the oxidative stress induced by H_2O_2 in BM-MSCs and following ROS production and apoptosis. Finally, it was shown that CeO_2 NPs could be used as potential antibacterial candidate, especially against gram-negative pathogens.

The binding responses of CeO_2 NPs with biomolecules are important features in understanding the toxicity and bioavailability of CeO_2 NPs in biological systems. In the future, we can also explore the effect of several parameters such as the dimension, functional groups and chemical composition of NPs, promoting the examination of the impact of different factors on the binding characteristics of NP-protein complexes as well as antioxidant and antibacterial properties of NPs. This study may provide useful data regarding the safe and potential implementation of NPs in biological systems.

Disclosure

The authors report no conflicts of interest in this work.

Acknowledgement

The financial support of Tehran Medical Sciences, Islamic Azad University, Tehran, Iran is greatly acknowledged.

References

[1] X. Gong, D. Huang, Y. Liu, Z. Peng, G. Zeng, P. Xu, M. Cheng, R. Wang, J. Wan, Remediation of contaminated soils by biotechnology with nanomaterials: bio-behavior, applications, and perspectives, Crit. Rev. Biotechnol. 38 (3) (2018) 455–468. Apr 3.
[2] M. Hofmann-Amtenbrink, D.W. Grainger, H. Hofmann, Nanoparticles in medicine: current challenges facing inorganic nanoparticle toxicity assessments and standardizations, Nanomed. Nanotechnol. Biol. Med. 11 (7) (2015) 1689–1694. Oct 1.
[3] C. Gaucher, A. Boudier, J. Bonetti, I. Clarot, P. Leroy, M. Parent, Glutathione: antioxidant properties dedicated to nanotechnologies, Antioxidants 7 (5) (2018) 62–69. May.
[4] T. Kim, Q. Zhang, J. Li, L. Zhang, J.V. Jokerst, A gold/silver hybrid nanoparticle for treatment and photoacoustic imaging of bacterial infection, ACS Nano 12 (6) (2018) 5615–5625. May 10.
[5] L.C. Lin, S. Chattopadhyay, J.C. Lin, C.M. Hu, Advances and opportunities in nanoparticle-and nanomaterial-based vaccines against bacterial infections, Adv. Healthc. Mater. 7 (13) (2018) 1701395–1701399. Jul.
[6] T. Lin, P. Zhao, Y. Jiang, Y. Tang, H. Jin, Z. Pan, H. He, V.C. Yang, Y. Huang, Blood–brain-barrier-penetrating albumin nanoparticles for biomimetic drug delivery via albumin-binding protein pathways for antiglioma therapy, ACS Nano 10 (11) (2016) 9999–10012. Nov 8.
[7] A. Trounson, C. McDonald, Stem cell therapies in clinical trials: progress and challenges, Cell Stem Cell 17 (1) (2015) 11–22. Jul 2.
[8] Q. Liu, M.X. Chen, L. Sun, C.U. Wallis, J.S. Zhou, L.J. Ao, Q. Li, P.C. Sham, Rational use of mesenchymal stem cells in the treatment of autism spectrum disorders, World J. Stem Cells 11 (2) (2019) 55–65. Feb 26.
[9] C. Vissers, G.L. Ming, H. Song, Nanoparticle technology and stem cell therapy team up against neurodegenerative disorders, Adv. Drug Deliv. Rev. 1 (1) (2019) 1–10. Feb 21.
[10] A. Gupta, S. Mumtaz, C.H. Li, I. Hussain, V.M. Rotello, Combatting antibiotic-resistant bacteria using nanomaterials, Chem. Soc. Rev. 48 (2) (2019) 415–427.
[11] C. Xu, X. Qu, Cerium oxide nanoparticle: a remarkably versatile rare earth nanomaterial for biological applications, NPG Asia Mater. 6 (3) (2014) e90–99. Mar.
[12] S. Das, J.M. Dowding, K.E. Klump, J.F. McGinnis, W. Self, S. Seal, Cerium oxide nanoparticles: applications and prospects in nanomedicine, Nanomedicine 8 (9) (2013) 1483–1508. Sep.
[13] Y.S. Khadar, A. Balamurugan, V.P. Devarajan, R. Subramanian, S.D. Kumar, Synthesis, characterization and antibacterial activity of cobalt doped cerium oxide (CeO2: Co) nanoparticles by using hydrothermal method, J. Mater. Res. Technol. 8 (1) (2019) 267–274. Jan 1.
[14] F.A. Olgun, A. Üzer, B.D. Ozturk, R. Apak, A novel cerium oxide nanoparticles–based colorimetric sensor using tetramethyl benzidine reagent for antioxidant activity assay, Talanta 182 (2018) 55–61. May 15.
[15] S.M. Hirst, A.S. Karakoti, R.D. Tyler, N. Sriranganathan, S. Seal, C.M. Reilly, Anti-inflammatory properties of cerium oxide nanoparticles, Small 5 (24) (2009) 2848–2856. Dec 18.
[16] M.S. Wason, J. Zhao, Cerium oxide nanoparticles: potential applications for cancer and other diseases, Am. J. Transl. Res. 5 (2) (2013) 126–133.
[17] P. Bellio, C. Luzi, A. Mancini, S. Cracchiolo, M. Passacantando, L. Di Pietro, M. Perilli, G. Amicosante, S. Santucci, G. Celenza, Cerium oxide nanoparticles as potential antibiotic adjuvant. Effects of CeO2 nanoparticles on bacterial outer membrane permeability, Biochim. Biophys. Acta Biomembr. 1860 (11) (2018) 2428–2435. Nov 1.
[18] P. Eriksson, A.A. Tal, A. Skallberg, C. Brommesson, Z. Hu, R.D. Boyd, W. Olovsson, N. Fairley, I.A. Abrikosov, X. Zhang, K. Uvdal, Cerium oxide nanoparticles with antioxidant capabilities and gadolinium integration for MRI contrast enhancement, Sci. Rep. 8 (1) (2018) 6999–7005. May 3.
[19] H.A. Zeinabad, E. Kachooei, A.A. Saboury, I. Kostova, F. Attar, M. Vaezzadeh, M. Falahati, Thermodynamic and conformational changes of protein toward interaction with nanoparticles: a spectroscopic overview, RSC Adv. 6 (107) (2016) 105903–105919.
[20] N. Eskandari, M.M. Babadaei, S. Nikpur, G. Ghasrahmad, F. Attar, M. Heshmati, K. Akhtari, S.M. Sorkhabadi, S.E. Mousavi, M. Falahati, Biophysical, docking, and cellular studies on the effects of cerium oxide nanoparticles on blood components: in vitro, Int. J. Nanomed. 13 (2018) 4575–4585.
[21] N.S. Pagadala, K. Syed, J. Tuszynski, Software for molecular docking: a review, Biophys. Rev. 9 (2) (2017) 91–102. Apr 1.
[22] A. Pourgholaminejad, N. Aghdami, H. Baharvand, S.M. Moazzeni, The effect of pro-inflammatory cytokines on immunophenotype, differentiation capacity and immunomodulatory functions of human mesenchymal stem cells, Cytokine 85 (2016) 51–60. Sep. 1.
[23] B. Ahmad, S. Parveen, R.H. Khan, Effect of albumin conformation on the binding of ciprofloxacin to human serum albumin: a novel approach directly assigning binding site, Biomacromolecules 7 (4) (2006) 1350–1356. Apr 10.
[24] S.K. Chaturvedi, E. Ahmad, J.M. Khan, P. Alam, M. Ishtikhar, R.H. Khan, Elucidating the interaction of limonene with bovine serum albumin: a multi-technique approach, Mol. Biosyst. 11 (1) (2015) 307–316.
[25] P. Alam, S.K. Chaturvedi, T. Anwar, M.K. Siddiqi, M.R. Ajmal, G. Badr, M.H. Mahmoud, R.H. Khan, Biophysical and molecular docking insight into the interaction of cytosine β-D arabinofuranoside with human serum albumin, J. Lumin. 164 (2015) 123–130. Aug 1.
[26] P. Alam, A.S. Abdelhameed, R.K. Rajpoot, R.H. Khan, Interplay of multiple interaction forces: binding of tyrosine kinase inhibitor nintedanib with human serum albumin, J. Photochem. Photobiol. B Biol. 157 (2016) 70–76. Apr 1.
[27] M.R. Ajmal, F. Almutairi, N. Zaidi, P. Alam, M.K. Siddiqi, M.V. Khan, M. Zaman, M. Ishtikhar, R.H. Khan, Biophysical insights into the interaction of clofazimine with human alpha 1-acid glycoprotein: a multitechnique approach, J. Biomol. Struct. Dyn. 37 (6) (2019) 1390–1401. Apr 13.
[28] R. Agrawal, Y. Thakur, M. Tripathi, M.K. Siddiqi, R.H. Khan, R. Pande, Elucidating the binding propensity of naphthyl hydroxamic acid to human serum albumin (HSA): multi-spectroscopic and molecular modeling approach, J. Mol. Struct. 1184 (2019) 1–10. May 15.
[29] M. Zaman, H.A. Safdari, A.N. Khan, S.M. Zakariya, S. Nusrat, T.I. Chandel, R.H. Khan, Interaction of anticancer drug pinostrobin with lysozyme: a biophysical and molecular docking approach, J. Biomol. Struct. Dyn. (2019) 1–7. Jan 8.
[30] A. Micsonai, F. Wien, J. Kun, H. Vadászi, M. Réfrégiers, J. Kardos, Protein fold recognition by circular dichroism spectroscopy, Biophys. J. 114 (3) (2018) 174–175. Feb 2.
[31] S. Awasthi, R. Preethy, N.T. Saraswathi, Nordihydroguaiaretic acid prevents glycation induced structural alterations and aggregation of albumin, Int. J. Biol. Macromol. 122 (2019) 479–484. Feb 1.
[32] M. Sedighipoor, A.H. Kianfar, W.A. Mahmood, M.H. Azarian, Synthesis and electronic structure of novel schiff bases Ni/Cu (II) complexes: evaluation of DNA/Serum protein binding by spectroscopic studies, Polyhedron 129 (2017) 1–8. Jun 17.
[33] M. Song, S. Liu, J. Yin, H. Wang, Interaction of human serum album and C60 aggregates in solution, Int. J. Mol. Sci. 12 (8) (2011) 4964–4974. Aug.
[34] S. Huang, H. Qiu, S. Lu, F. Zhu, Q. Xiao, Study on the molecular interaction of graphene quantum dots with human serum albumin: combined spectroscopic and electrochemical approaches, J. Hazard Mater. 285 (2015) 18–26. Mar 21.
[35] L. Lai, C. Lin, Z.Q. Xu, X.L. Han, F.F. Tian, P. Mei, D.W. Li, Y.S. Ge, F.L. Jiang,

Y.Z. Zhang, Y. Liu, Spectroscopic studies on the interactions between CdTe quantum dots coated with different ligands and human serum albumin, Spectrochim. Acta A Mol. Biomol. Spectrosc. 97 (2012) 366–376. Nov 1.
[36] L. Treuel, M. Malissek, J.S. Gebauer, R. Zellner, The influence of surface composition of nanoparticles on their interactions with serum albumin, ChemPhysChem 11 (14) (2010) 3093–3099. Oct 4.
[37] A. Ansari, S. Sachar, S.S. Garje, Synthesis of bare and surface modified TiO_2 nanoparticles via a single source precursor and insights into their interactions with serum albumin, New J. Chem. 42 (16) (2018) 13358–13366.
[38] A. Maji, M. Beg, A.K. Mandal, S. Das, P.K. Jha, A. Kumar, S. Sarwar, M. Hossain, P. Chakrabarti, Spectroscopic interaction study of human serum albumin and human hemoglobin with Mersilea quadrifolia leaves extract mediated silver nanoparticles having antibacterial and anticancer activity, J. Mol. Struct. 1141 (2017) 584–592. Aug 5.
[39] S. Ambika, M. Sundrarajan, Green biosynthesis of ZnO nanoparticles using Vitex negundo L. extract: spectroscopic investigation of interaction between ZnO nanoparticles and human serum albumin, J. Photochem. Photobiol. B Biol. 149 (2015) 143–148. Aug 1.
[40] M.S. Ali, H.A. Al-Lohedan, A.M. Atta, A.O. Ezzat, S.A. Al-Hussain, Interaction of human serum albumin with silver nanoparticles functionalized with polyvinylthiol, J. Mol. Liq. 204 (2015) 248–254. Apr 1.
[41] S. Naveenraj, R.V. Mangalaraja, O. Krasulyaa, A. Syed, F. Ameen, S. Anandan, A general microwave synthesis of metal (Ni, Cu, Zn) selenide nanoparticles and their competitive interaction with human serum albumin, New J. Chem. 42 (8) (2018) 5759–5766.
[42] D. Shcharbin, E. Pedziwiatr-Werbicka, T. Serchenya, S. Cyboran-Mikolajczyk, L. Prakhira, V. Abashkin, V. Dzmitruk, M. Ionov, S. Loznikova, I. Shyrochyna, O. Sviridov, Role of cationic carbosilane dendrons and metallic core of functionalized gold nanoparticles in their interaction with human serum albumin, Int. J. Biol. Macromol. 118 (2018) 1773–1780. Oct 15.
[43] H.A. Rather, R. Thakore, R. Singh, D. Jhala, S. Singh, R. Vasita, Antioxidative study of Cerium Oxide nanoparticle functionalised PCL-Gelatin electrospun fibers for wound healing application, Bioactive Mater. 3 (2) (2018) 201–211. Jun 1.
[44] Y. Xue, S.R. Balmuri, A. Patel, V. Sant, S. Sant, Synthesis, physico-chemical characterization, and antioxidant effect of PEGylated cerium oxide nanoparticles, Drug Deliv. Transl. Res. 8 (2) (2018) 357–367. Apr 1.
[45] P. Patel, K. Kansara, R. Singh, R.K. Shukla, S. Singh, A. Dhawan, A. Kumar, Cellular internalization and antioxidant activity of cerium oxide nanoparticles in human monocytic leukemia cells, Int. J. Nanomed. 13 (2018) 39–40.
[46] N.J. Abuid, K.M. Gattás-Asfura, E.A. Schofield, C.L. Stabler, Layer-by-Layer cerium oxide nanoparticle coating for antioxidant protection of encapsulated Beta cells, Adv. Healthc. Mater. (2019) 1801493–1801499. Jan 11.
[47] A. Filippi, F. Liu, J. Wilson, S. Lelieveld, K. Korschelt, T. Wang, Y. Wang, T. Reich, U. Pöschl, W. Tremel, H. Tong, Antioxidant activity of cerium dioxide nanoparticles and nanorods in scavenging hydroxyl radicals, RSC Adv. 9 (20) (2019) 11077–11081.
[48] S. Del Turco, G. Ciofani, V. Cappello, P. Parlanti, M. Gemmi, C. Caselli, R. Ragusa, A. Papa, D. Battaglia, L. Sabatino, G. Basta, Effects of cerium oxide nanoparticles on hemostasis: coagulation, platelets and vascular endothelial cells, J. Biomed. Mater. Res. A 1 (2019) 1–10. Mar 18.
[49] A. Pesaraklou, N. Mahdavi-Shahri, H. Hassanzadeh, M. Ghasemi, M. Kazemi, N.S. Mousavi, M.M. Matin, Use of cerium oxide nanoparticles: a good candidate to improve skin tissue engineering, Biomed. Mater. 1 (2019) 1–10. Feb 12.
[50] A. Lopez-Pascual, A. Urrutia-Sarratea, S. Lorente-Cebrián, J.A. Martinez, P. González-Muniesa, Cerium oxide nanoparticles regulate insulin sensitivity and oxidative markers in 3T3-L1 adipocytes and C2C12 myotubes, Oxid. Med. Cell. Longev. 1 (2019) 1–10.
[51] Y. Li, X. Hou, C. Yang, Y. Pang, X. Li, G. Jiang, Y. Liu, Photoprotection of Cerium oxide Nanoparticles against UVA radiation-induced senescence of Human skin Fibroblasts due to their Antioxidant properties, Sci. Rep. 9 (1) (2019) 2595–2599. Feb 22.
[52] B. Lu, D.Y. Zhu, J.H. Yin, H. Xu, C.Q. Zhang, Q.F. Ke, Y.S. Gao, Y.P. Guo, Incorporation of cerium oxide in hollow mesoporous bioglass scaffolds for enhanced bone regeneration by activating the ERK signaling pathway, Biofabrication 11 (2) (2019) 025012–025022. Mar 28.
[53] C. Zgheib, S.A. Hilton, L.C. Dewberry, M.M. Hodges, S. Ghatak, J. Xu, S. Singh, S. Roy, C.K. Sen, S. Seal, K.W. Liechty, Use of cerium oxide nanoparticles conjugated with MicroRNA-146a to correct the diabetic wound healing impairment, J. Am. Coll. Surg. 228 (1) (2019) 107–115. Jan 1.
[54] A. Asati, S. Santra, C. Kaittanis, S. Nath, J.M. Perez, Oxidase-like activity of polymer-coated cerium oxide nanoparticles, Angew. Chem. Int. Ed. 48 (13) (2009) 2308–2312. Mar 16.
[55] C. Korsvik, S. Patil, S. Seal, W.T. Self, Superoxide dismutase mimetic properties exhibited by vacancy engineered ceria nanoparticles, Chem. Commun. (10) (2007) 1056–1058.
[56] A. Arya, A. Gangwar, M. Das, K. Bhargava, Nanozyme and antioxidant mimetic cerium oxide nanoparticles confer excellent protection against UV induced oxidative damage in skin, Free Radic. Biol. Med. 100 (2016) S92–S93. Nov 1.
[57] S. Singh, Cerium oxide based nanozymes: redox phenomenon at biointerfaces, Biointerphases 11 (4) (2016), 04B202. Dec 2-10.
58 R. Singh, S. Singh, Redox-dependent catalase mimetic cerium oxide-based nanozyme protect human hepatic cells from 3-AT induced acatalasemia, Colloids Surfaces B Biointerfaces 175 (2019) 625–635. Mar 1.
[59] A. Filippi, F. Liu, J. Wilson, S. Lelieveld, K. Korschelt, T. Wang, Y. Wang, T. Reich, U. Pöschl, W. Tremel, H. Tong, Antioxidant activity of cerium dioxide nanoparticles and nanorods in scavenging hydroxyl radicals, RSC Adv. 9 (20) (2019) 11077–11081.
[60] O. Zeyons, A. Thill, F. Chauvat, Direct and indirect CeO2 nanoparticles toxicity for Escherichia coli and Synechocystis, Nanotoxicology 3 (2009) 284–295.
[61] D.A. Pelletier, A.K. Suresh, G.A. Holton, C.K. McKeown, W. Wang, B. Gu, N.P. Mortensen, D.P. Allison, D.C. Joy, M.R. Allison, S.D. Brown, T.J. Phelps, M.J. Doktycz, Effects of engineered cerium oxide nanoparticles on bacterial growth and viability, Appl. Environ. Mirobiol. 76 (24) (2010) 7981–7989. Dec.
[62] Y. Kuang, X. He, Z. Zhang, Y. Li, H. Zhang, et al., Comparison study on the antibacterial activity of nano- or bulk-cerium oxide, J. Nanosci. Nanotechnol. 11 (2011) 4103–4108.
[63] K. Gopinath, V. Karthika, C. Sundaravadivelan, S. Gowri, A. Arumugam, Mycogenesis of cerium oxide nanoparticles using Aspergillus Niger culture filtrate and their applications for antibacterial and larvicidal activities, J. Nanostruct. Chem. 5 (2015) 295–303.
[64] J. Malleshappa, H. Nagabhushana, S.C. Sharma, Y.S. Vidya, K.S. Anantharaju, S.C. Prashantha, B. Daruka Prasad, H. Raja Naika, K. Lingaraju, B.S. Surendra, Leucas aspera mediated multifunctional CeO2 nanoparticles: structural, photoluminescent, photocatalytic and antibacterial properties, Spectrochim. Acta A Mol. Biomol. Spectrosc. 149 (2015) 452–462.
[65] N. Padmavathy, R. Vijayaraghavan, Enhanced bioactivity of ZnO nanoparticles—an antimicrobial study, Sci. Technol. Adv. Mater. 9 (3) (2008), 035004. -10.
[66] S. Haq, W. Rehman, M. Waseem, R. Javed, M. Shahid, Effect of heating on the structural and optical properties of TiO 2 nanoparticles: antibacterial activity, Appl. Nanosci. 8 (1–2) (2018) 11–18. Feb 1.
[67] B. Peng, X. Zhang, D.G. Aarts, R.P. Dullens, Superparamagnetic nickel colloidal nanocrystal clusters with antibacterial activity and bacteria binding ability, Nat. Nanotechnol. 13 (6) (2018) 478–485. Jun.
[68] L.L. Duffy, M.J. Osmond-McLeod, J. Judy, T. King, Investigation into the antibacterial activity of silver, zinc oxide and copper oxide nanoparticles against poultry-relevant isolates of Salmonella and Campylobacter, Food Control 92 (2018) 293–300. Oct 1.
[69] W.R. Rolim, M.T. Pelegrino, B. de Araújo Lima, L.S. Ferraz, F.N. Costa, J.S. Bernardes, T. Rodigues, M. Brocchi, A.B. Seabra, Green tea extract mediated biogenic synthesis of silver nanoparticles: characterization, cytotoxicity evaluation and antibacterial activity, Appl. Surf. Sci. 463 (2019) 66–74. Jan 1.
[70] Z. Song, Y. Wu, H. Wang, H. Han, Synergistic antibacterial effects of curcumin modified silver nanoparticles through ROS-mediated pathways, Mater. Sci. Eng. C 99 (2019) 255–263. Jun 1.
71 K.S. Siddiqi, A. ur Rahman, A. Husen, Properties of zinc oxide nanoparticles and their activity against microbes, Nanoscale Res. Lett. 13 (1) (2018) 141–150. Dec.
[72] H. Yang, C. Liu, D. Yang, H. Zhang, Z. Xi, Comparative study of cytotoxicity, oxidative stress and genotoxicity induced by four typical nanomaterials: the role of particle size, shape and composition, J. Appl. Toxicol. 29 (1) (2009) 69–78.
[73] M. Hoseinnejad, S.M. Jafari, I. Katouzian, Inorganic and metal nanoparticles and their antimicrobial activity in food packaging applications, Crit. Rev. Microbiol. 44 (2) (2018) 161–181. Mar 4.
[74] Q. Lv, B. Zhang, X. Xing, Y. Zhao, R. Cai, W. Wang, Q. Gu, Biosynthesis of copper nanoparticles using Shewanella loihica PV-4 with antibacterial activity: novel approach and mechanisms investigation, J. Hazard Mater. 347 (2018) 141–149. Apr 5.
[75] F.K. Alsammarraie, W. Wang, P. Zhou, A. Mustapha, M. Lin, Green synthesis of silver nanoparticles using turmeric extracts and investigation of their antibacterial activities, Colloids Surfaces B Biointerfaces 171 (2018) 398–405. Nov 1.
[76] V. Pareek, R. Gupta, J. Panwar, Do physico-chemical properties of silver nanoparticles decide their interaction with biological media and bactericidal action? A review, Mater. Sci. Eng. C 90 (2018) 739–749. Sep. 1.
[77] W. Pajerski, D. Ochonska, M. Brzychczy-Wloch, P. Indyka, M. Jarosz, M. Golda-Cepa, Z. Sojka, A. Kotarba, Attachment efficiency of gold nanoparticles by Gram-positive and Gram-negative bacterial strains governed by surface charges, J. Nanoparticle Res. 21 (8) (2019) 186–195. Aug 1.
[78] A.F. Halbus, T.S. Horozov, V.N. Paunov, Strongly enhanced antibacterial action of copper oxide nanoparticles with boronic acid surface functionality, ACS Appl. Mater. Interfaces 11 (13) (2019) 12232–12243. Mar 20.
[79] F. Qin, T. Shen, J. Li, J. Qian, J. Zhang, G. Zhou, J. Tong, SF-1 mediates reproductive toxicity induced by Cerium oxide nanoparticles in male mice, J. Nanobiotechnol. 17 (1) (2019) 41–50. Dec.
[80] R. Liman, Y. Acikbas, İ.H. Ciğerci, Cytotoxicity and genotoxicity of cerium oxide micro and nanoparticles by Allium and Comet tests, Ecotoxicol. Environ. Saf. 168 (2019) 408–414. Jan 30.